IEEE Photonics Journal
An IEEE Photonics Society Publication

Dynamics of Self-Heating in Microring Resonators

Volume 4, Number 5, October 2012

Amir Arbabi, Student Member, IEEE
Lynford L. Goddard, Senior Member, IEEE

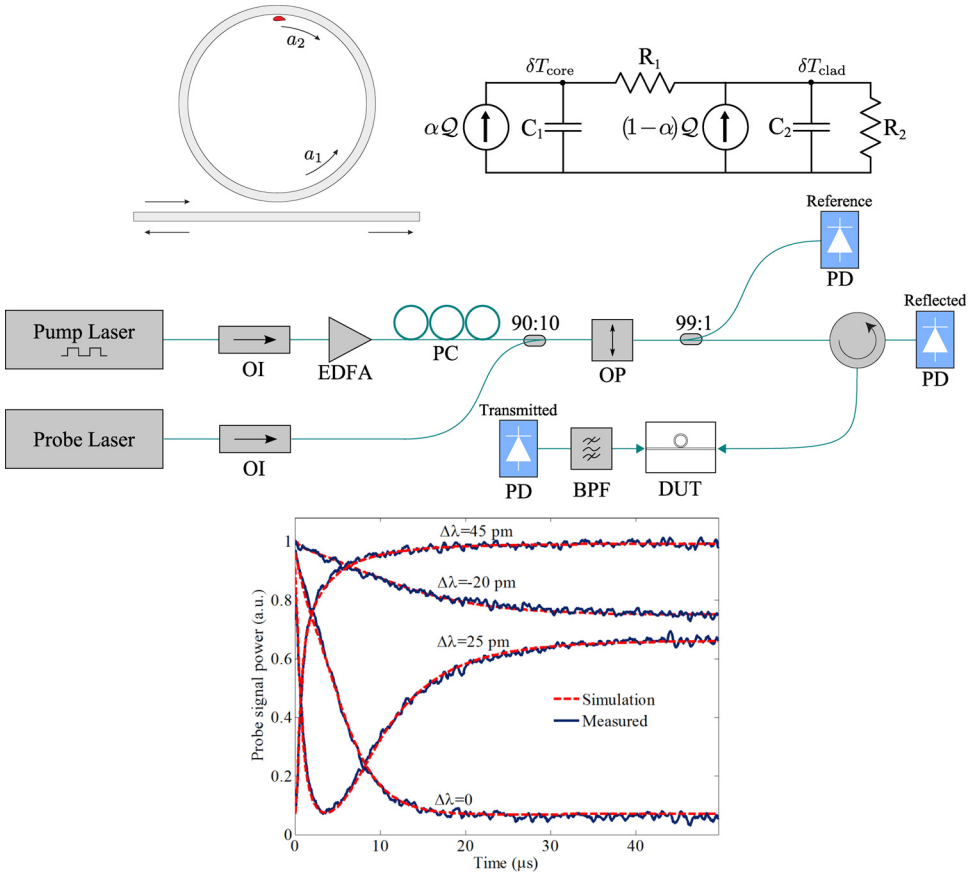

DOI: 10.1109/JPHOT.2012.2214205
1943-0655/$31.00 ©2012 IEEE

Dynamics of Self-Heating in Microring Resonators

Amir Arbabi, *Student Member, IEEE*, and Lynford L. Goddard, *Senior Member, IEEE*

Department of Electrical and Computer Engineering, Micro and Nanotechnology Laboratory, University of Illinois at Urbana-Champaign, Urbana, IL 61801 USA

DOI: 10.1109/JPHOT.2012.2214205
1943-0655/$31.00 ©2012 IEEE

Manuscript received June 28, 2012; revised August 14, 2012; accepted August 16, 2012. Date of publication August 20, 2012; date of current version September 4, 2012. This work was supported in part by the University of Illinois startup funds and in part by the National Science Foundation CAREER award ECCS-1055941. Corresponding author: L. L. Goddard (e-mail: lgoddard@illinois.edu).

Abstract: We theoretically and experimentally study the dynamics of self-heating in microring resonators. We present a coupled thermal and optical model based on a lumped capacitance thermal model and optical time-domain coupled-mode theory, and verify it using experimental measurements. The thermal dynamics are modeled by a second-order linear system, and the optical model considers the coupling between the two degenerate counter propagating modes of the microring resonator. The two models are coupled through the stored optical energy inside the microring resonator. The self-heating dynamics are measured using direct and pump-probe methods, and the results of both techniques are in good agreement with the proposed theoretical model.

Index Terms: Waveguide devices, nanophotonics, integrated nanophotonic systems.

1. Introduction

Optical power loss caused by material absorption reduces the quality factor of integrated optical resonators. The absorbed optical power is converted to heat, which changes the temperature of the resonator. The temperature change alters the resonator's material refractive index through the thermooptic effect and moves its resonant wavelength. As the resonant wavelength moves, the optical energy stored in the resonator, the amount of absorbed optical energy, and the generated heat all vary. Therefore, self-heating and the thermooptic effect couple the thermal and optical dynamics of the resonator. For constant input optical power, the generated heat, the resonator temperature change, and the index change due to the thermooptic effect are proportional to the optical power in the resonator. Therefore, the combined self-heating and thermooptic effects lead to an intensity-dependent refractive index. Resonators with an intensity-dependent refractive index are known to have bistable relations between the input and output powers [1].

Several methods for either decreasing [2], [3] or increasing [4], [5] the optical power required to observe the thermally induced resonance shift and nonlinearity have been reported. Thermally induced bistability has been observed in silicon-on-insulator (SOI) microrings with powers as low as tens of microwatts [2], [6], [7]. Silicon nitride is a CMOS process compatible material, and due to its relatively high contrast to silicon dioxide, it can be used for the realization of relatively small passive integrated optic devices. In the telecommunication band, silicon nitride microrings have lower optical absorption loss [mostly caused by Si-H and N-H bonds in Si_3N_4 and SiO_2 grown by plasma-enhanced chemical vapor deposition (PECVD)] and a smaller thermooptic coefficient than silicon. As a result, a few milliwatts of optical input power is required for observation of thermally induced

optical nonlinearity [8] and bistability [9] in silicon nitride on SiO_2 microrings. Devices utilizing thermally induced optical bistability in microresonators are mostly intended for applications in all-optical signal processing; switches and memories have been already demonstrated [6], [10]. In silicon nitride microrings, the thermally induced nonlinearity is relatively large compared with the Kerr nonlinearity, but its main drawback is its slow response, which limits the bandwidth of these devices to a few MHz. On the other hand, the prime advantage of all-optical processing over its electronic and optoelectronic counterparts is its potential for extremely large bandwidth. Therefore, the use of thermally induced nonlinearity for all-optical data processing is not well justified. Nevertheless, the optical nonlinearity affects the functional response of microresonators in low-frequency applications.

One set of devices that are expected to be affected by thermally induced nonlinearity is reflective microrings. Reflective microrings are a family of microresonator-based devices that work based on selectively coupling degenerate counter propagating modes of a microring resonator by integrating a reflector on the microring's waveguide. Reflective microrings with several types of reflection spectra such as a single wavelength narrowband reflector, and comb of reflection peaks with different reflectivities have been proposed [11] and demonstrated [12]. These devices have been proposed to replace the conventional linear distributed Bragg reflectors (DBRs) and sampled grating DBRs that are used as the cavity mirrors of semiconductor laser diodes [13]. A nonlinear reflectivity response and bistability in reflective microrings can affect the performance of laser diodes that use these devices as cavity mirrors. Understanding the dynamic response of the reflector is critical for meeting functional requirements, especially in tunable applications. The direct large signal modulation response of the laser also depends on the time-domain response of the microring reflector. Furthermore, the dependence of the reflection peak wavelength of the microring reflector on the optical power converts the laser's intensity noise to phase noise. In other words, fluctuations in the laser power lead to fluctuations in the phase of the reflectivity of the reflective microring and can affect the laser linewidth and lineshape.

Here, we present a theoretical model that describes the dynamics of mutual thermal and optical coupling caused by self-heating and thermooptic effects in microring resonators. Because of the application of the presented model to reflective microrings, we consider the more general case of microrings with coupling between counter propagating degenerate modes. In Section 2, we present a time-domain coupled-mode-based method for modeling coupling between two counter propagating degenerate modes of a microring with small perturbations. In Section 3, we introduce a second-order lumped capacitance thermal model for microrings by approximating its thermal response by a summation of two exponential functions. We also couple the dynamic optical and thermal models and provide a nonlinear ordinary differential equation, which describes the temporal dynamics of the resonant frequency of the microring. We fabricated silicon nitride on SiO_2 microrings and characterized self-heating dynamics by performing direct and pump-probe measurements. The measurement results are presented in Section 5 and are compared to the simulation results of the model. Good agreement between the experimental results and the theoretical model is achieved, which supports the validity of the model. Further, inclusion of the mutual coupling between degenerate modes and two thermal time constants in the model is critical for the good agreement.

2. Time-Domain Modeling of Microring Resonators

Time-domain dynamics of a system of coupled lumped resonators can be modeled using time-domain coupled-mode theory (TDCMT) [14]. In this method, the field amplitude of the ith resonator is represented using its energy amplitude $a_i(t)$ so that the energy stored in the ith resonator is $|a_i(t)|^2$. The phase of the energy amplitude can be chosen to be the same as the phase of the electric field of the resonator. TDCMT provides a system of linear coupled first-order ordinary differential equations, which can exactly model the dynamics of such a system of lumped resonators. The TDCMT can also be used to model a system of coupled distributed resonators. Distributed resonators have infinite resonance modes, and the use of the TDCMT usually involves using a finite number of them whose resonance frequencies fall inside the bandwidth of interest.

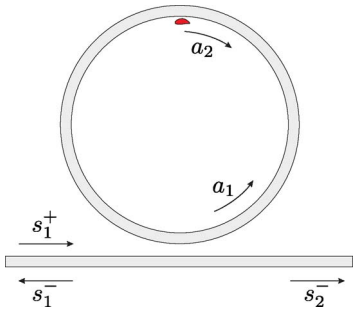

Fig. 1. Microring resonator with coupled degenerate counter propagating modes. a_1 and a_2 represent the energy amplitudes of the counterclockwise and clockwise modes, respectively. $s_i^{\pm}$ are the power amplitudes in the input and output waveguides.

Therefore, TDCMT provides an accurate and fast model for a system as long as the bandwidth of signals of interest contains a small number of the resonators' resonant modes. This condition usually holds in the case of an integrated optics resonator with a free spectral range of few nanometers since the signal bandwidth of the laser is usually less than a nanometer.

For the case of a microring resonator with an input signal bandwidth less than its free spectral range, we only need to consider the two degenerate counter propagating modes within the signal bandwidth. When there is no coupling between these two modes, the temporal dynamics of the energy amplitudes of these modes are given by

$$\frac{da_1}{dt} = j\omega_0 a_1 - \frac{a_1}{\tau} + \kappa s_1^+ \tag{1a}$$

$$\frac{da_2}{dt} = j\omega_0 a_2 - \frac{a_2}{\tau} \tag{1b}$$

where ω_0 is the resonance frequency of the modes and s_1^+ represents the power amplitude of the forward propagating wave in the bus waveguide. τ represents the decay time of the modes due to material and radiation losses and decoupling to the bus waveguide, and κ is a coefficient expressing the coupling strength to the bus waveguide. A small perturbation (see Fig. 1) to the ideal microring can couple its two degenerate modes, and the TDCMT equations become

$$\frac{da_1}{dt} = j\omega_0 a_1 + j\kappa_m a_2 - \frac{a_1}{\tau} + \kappa s_1^+ \tag{2a}$$

$$\frac{da_2}{dt} = j\omega_0 a_2 + j\kappa_m a_1 - \frac{a_2}{\tau} \tag{2b}$$

where κ_m coefficient represents the coupling strength of the two modes. The transmitted and reflected power amplitudes are related to the energy amplitudes of the modes as

$$s_2^- = -s_1^+ + \kappa a_1 \tag{3a}$$

$$s_1^- = \kappa a_2. \tag{3b}$$

It should be noted that the phase reference for the power amplitudes can be chosen arbitrarily. These phases have been chosen such that (1)–(3) are symmetric with respect to the two microring modes. Theoretical estimates for microring optical parameters can be found in the literature [14], [15]; τ is directly related to the microring's quality factor, κ_m is determined by the sidewall roughness, and κ depends critically on the gap size. However, for greatest model accuracy, we will find these parameters experimentally in Section 5 by fitting our optical model results to the measured spectra at low power where thermal effects are negligible.

According to (2), the energy amplitudes reach their steady-state values on a time scale on the order of the decay time (τ). Even for microring resonators with loaded quality factors as high as on the order of 10^6, the decay time is in the subnanosecond range. Considering the microsecond

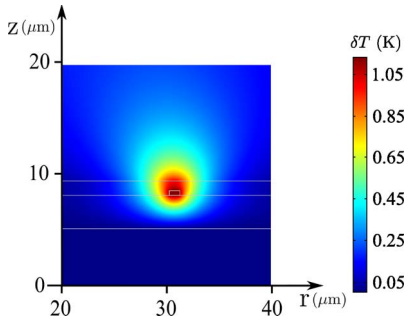

Fig. 2. Steady-state distribution of temperature change on the cross section of a Si_3N_4 microring resonator found using FEM simulation. A heat source with uniform density of 10^{-2} mW/$(\mu m)^3$ is assumed in the microring core.

thermal transient time constants of the microring resonators, we can use an adiabatic approximation for evaluating the mode energy amplitudes and assume their steady-state values during thermal transience. Frequency-domain steady-state values of the microring modes' energy amplitudes excited by a laser at frequency of ω_l can also be found from (2) as

$$a_1 = \frac{-\left(j(\omega_0 - \omega_l) - \frac{1}{\tau}\right)\kappa}{(j(\omega_0 - \omega_l) - 1/\tau)^2 + \kappa_m^2} s_1^+ \tag{4a}$$

$$a_2 = \frac{j\kappa\kappa_m}{(j(\omega_0 - \omega_l) - 1/\tau)^2 + \kappa_m^2} s_1^+. \tag{4b}$$

As expected, the frequency domain spectrum has only two poles corresponding to the two resonance modes. The general frequency domain response of microring resonators with reflective elements is given in [11], which, when approximated in a narrow bandwidth around a resonant wavelength, leads to a similar form of response as (4).

3. Lumped Capacitance Thermal Model for Microring Resonators

To model the thermal dynamics of the microring, we performed a 3-D thermal simulation of a silicon nitride microring resonator using finite-element method (FEM). To model the thermal effects of optical material absorption, we assumed a constant uniform heat source in the silicon nitride core. The thermal conductivity of silicon nitride is about ten times that of silicon dioxide; therefore, the temperature is almost constant over the core region and the distribution of the heat source over the core does not significantly affect the results. The steady-state distribution of the temperature change over the microring's cross section is shown in Fig. 2. The average temperature of the Si_3N_4 core when we turn off the heat source and the microring cools down from its steady-state value is also found by FEM simulation and is represented in Fig. 3(a). For modeling the nonlinear response of the device due to self-heating, a simple but accurate model is needed. While FEM provides accurate thermal simulation results, it is not fast enough to be integrated with the optical model. On the other hand, the lumped capacitance method, which considers the device as a collection of lumped thermal masses exchanging heat through thermal resistors, can provide a fast and simple thermal model. Approximating diffusive heat transfer using a set of thermal capacitors and resistors is similar to lumped circuit elements' approximation of distributed electromagnetic systems (e.g., transmission lines). The accuracy of the results can be improved by adding more elements to the thermal circuit. As shown in Fig. 3(b), we used a lumped capacitance model with two thermal masses (represented by two thermal capacitors) for the microring's core and cladding regions and two thermal resistors to describe the thermal resistance between the core and cladding and between the cladding and ambient substrate and air. The total generated heat is assumed to be $\mathcal{Q}$ and is split into two portions, which are modeled by two heat sources in the thermal circuit. The heat

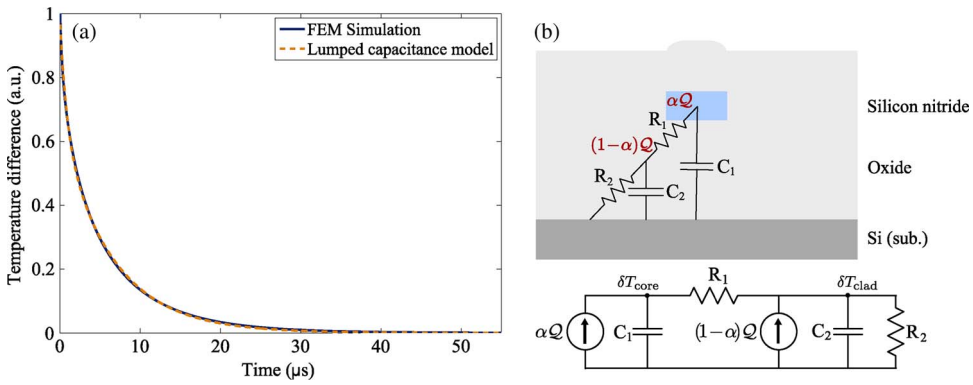

Fig. 3. (a) Average temperature difference between the Si_3N_4 core and its surroundings as a function of time. The solid line shows FEM simulation results while the dashed line represents the result from the lumped capacitance model with thermal masses. (b) Schematic diagram of a thermal circuit for modeling self-heating in microring resonators.

generated by light absorption in the core and cladding are represented by $\alpha\mathcal{Q}$ and $(1-\alpha)\mathcal{Q}$ heat sources, respectively, where $0 \leq \alpha \leq 1$ is the portion of heat generated in the core. The result of the second-order lumped thermal circuit of Fig. 3(b) for the core temperature change (δT_{core}) was fitted to the FEM simulation result and is overlaid on it in Fig. 3(a). The good agreement between the results suggests that the thermal dynamics of the microring can be modeled using the second-order lumped thermal circuit.

The impulse responses of the second-order circuit for the temperature changes of the core and cladding are given by

$$\delta T_{\text{core/clad}}(t) = A_{\text{core/clad}} e^{-t/t_1} + B_{\text{core/clad}} e^{-t/t_2} \tag{5}$$

where t_1 and t_2 are the time constants of the thermal response. The differential equations describing temporal dynamics of core and cladding temperature changes $(\delta T_{\text{core/clad}})$ are given by

$$\frac{d^2\delta T_{\text{core/clad}}}{dt^2} + \left(\frac{1}{t_1} + \frac{1}{t_2}\right)\frac{d\delta T_{\text{core/clad}}}{dt} + \frac{1}{t_1 t_2}\delta T_{\text{core/clad}} = \left(\frac{A_{\text{core/clad}}}{t_1} + \frac{B_{\text{core/clad}}}{t_2}\right)\frac{d\mathcal{Q}}{dt} + \frac{A_{\text{core/clad}} + B_{\text{core/clad}}}{t_1 t_2}\mathcal{Q}. \tag{6}$$

4. Dynamic Coupled Thermooptical Model

In Sections 2 and 3, we provided dynamic models for describing thermal and optical dynamics of microring resonators. In this section, we discuss mutual coupling between the thermal and optical dynamics caused by self-heating and thermooptic effects. Assuming linear optical material absorption, the generated heat in a microring is proportional to the stored optical energy in the microring, that is

$$\mathcal{Q} = \frac{1}{\tau_a}\left(|a_1|^2 + |a_2|^2\right) \tag{7}$$

where τ_a is the photon absorption life time and is related to the core and cladding material absorption coefficients. Although absorption in the core and cladding happen at different rates, the photon absorption life time refers to the total decay rate of the photon in the optical mode caused by material absorption. Note that the two microring resonator's counter propagating modes are orthogonal, and their energies add rather than their energy amplitudes. The thermally induced resonant frequency shift of the microring is linearly related to the core and cladding temperature change

$$\delta\omega_0 = -c_1\delta T_{\text{core}} - c_2\delta T_{\text{clad}} \tag{8}$$

where $c_{1,2}$ are coefficients related to the core and cladding material parameters, their thermooptic coefficients, and the optical confinement factor of the resonant mode. By combining (6)–(8), we can find the differential equation, which describes the temporal dynamics of the resonant frequency of a microring resonator as

$$\frac{d^2\delta\omega_0}{dt^2}+\left(\frac{1}{t_1}+\frac{1}{t_2}\right)\frac{d\delta\omega_0}{dt}+\frac{1}{t_1 t_2}\delta\omega_0=-\left(\frac{a}{t_1}+\frac{b}{t_2}\right)\frac{d\left(|a_1|^2+|a_2|^2\right)}{dt}-\frac{a+b}{t_1 t_2}\left(|a_1|^2+|a_2|^2\right). \quad (9)$$

The constant coefficients a and b are given by

$$a=\frac{c_1 A_{\text{core}}+c_2 A_{\text{clad}}}{\tau_a} \quad (10a)$$

$$b=\frac{c_1 B_{\text{core}}+c_2 B_{\text{clad}}}{\tau_a}. \quad (10b)$$

Lumped capacitance model parameters such as t_1, t_2, a, and b can be estimated by fitting the FEM numerical heat diffusion simulation results to those from the lumped model. Again, for greatest model accuracy, we will determine these parameters experimentally in Section 5 by fitting the data from the large signal modulation measurement or from the pump-probe experiment to the coupled thermooptical model.

As was mentioned in Section 2, we can use the adiabatic approximation for the energy amplitudes of the modes and replace them in (9) by their steady-state values from (4) using a time-dependent resonant frequency of $\omega_0(t)$. By making this substitution, (9) turns into a nonlinear differential equation for $\delta\omega_0(t)$ with $s_1^+(t)$ as the driving source. After finding the $\delta\omega_0(t)$, the transmitted and reflected power amplitudes can be found using (3) and (4).

5. Model Verification: Comparison With Experimental Results

We fabricated silicon nitride on silicon dioxide microring resonators and performed two sets of measurements to verify the validity of our model for describing the dynamics of self-heating. We measured time-domain waveforms of transmitted and reflected powers for large signal modulated laser input (direct measurement) and also carried out pump-probe measurements using two lasers.

The microrings were designed and fabricated with Si_3N_4 core and SiO_2 bottom and top claddings on a silicon substrate. A 3-μm-thick layer of SiO_2 was grown on a silicon substrate, and 400-nm-thick stoichiometric Si_3N_4 was deposited on the grown oxide using low-pressure chemical vapor deposition (LPCVD) technique. The microrings were patterned on the Si_3N_4 layer using e-beam lithography and reactive ion etching. To form the top cladding, a 1.3-μm-thick layer of SiO_2 was deposited on the patterned silicon nitride using PECVD. Waveguide facets were coated with 300-nm PECVD silicon diode to reduce their unwanted reflections. Microrings with 30-μm radius and 1-μm-wide waveguides with different coupling gaps were fabricated using this procedure.

Transmission and reflection spectra of the devices were measured at a low input power using a setup shown in Fig. 4. The average output power of the erbium-doped fiber amplifier (EDFA) was set to -5 dBm, and considering the 5 dB of coupling loss, the average power coupled to the device was estimated as $P_{\text{in}}=0.1$ mW. TE polarized light from a narrow linewidth tunable CW laser was coupled to the microrings' bus waveguide using a lensed fiber, and the transmitted signal was collected using a similar lensed fiber. The reflected optical power was measured using an optical circulator, which was placed before the input lensed fiber. The input power was monitored using a 99 : 1 optical coupler. A typical transmission and reflection spectrum of a microring resonator close to one of its resonances is shown in Fig. 5. The dip in the transmission spectrum close to the microring's resonance is accompanied by a reflection peak. The reflection is a result of coupling between the two degenerate counter propagating modes caused by a small amount of roughness of the microring waveguide. A time-domain coupled-mode model as in Section 2 was used for modeling the coupling between the two modes. Using the least-square fit to the measured data, the values of $\tau=64.7$ ps, $\kappa=1.5\times10^5$ s$^{-1/2}$, and $\kappa_m=6.2\times10^9$ s^{-1} were found for the energy

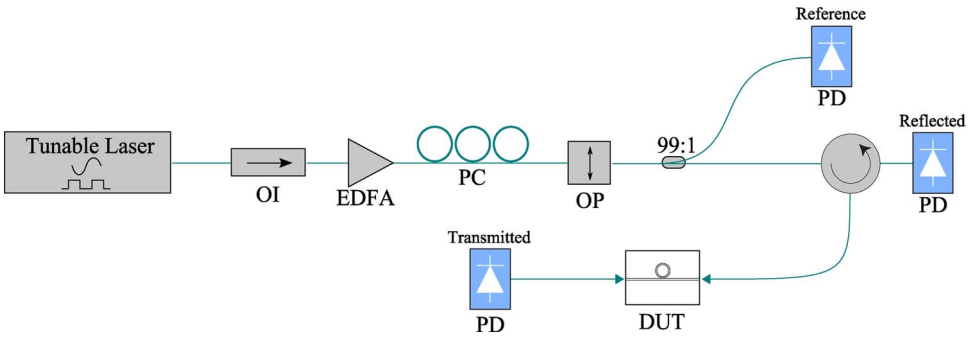

Fig. 4. Schematic of the experimental setup used for low power spectral measurements and direct nonlinear measurement with large signal modulation of the laser. For low power spectra measurements, the laser operated in CW mode and the EDFA's output power was set to −5 dBm, while the direct nonlinear measurement was performed with the laser modulated with 50% duty cycle and 100% modulation depth, and the EDFA's average output power of 16 dBm. OI: optical isolator, EDFA: erbium-doped fiber amplifier, PC: polarization controller, OP: optical polarizer, PD: photodetector, and DUT: device under test.

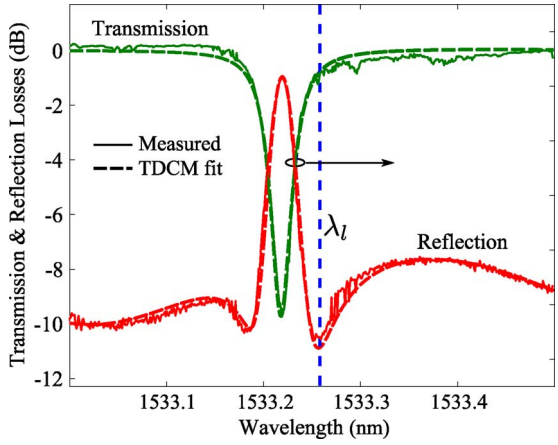

Fig. 5. Measured (solid lines) and TDCMT fit (dashed lines) to a typical transmission and reflection spectrum of a microring resonator close to one of its resonances. The dashed vertical line represents the laser excitation wavelength for the large signal modulation experiment of Fig. 6. As the microring resonator heats up due to the self-heating effect the transmission and reflection spectra red shift (as shown with an arrow).

amplitudes decay time, the bus to microring coupling coefficient, and coupling parameter between the modes, respectively. The loaded quality factor of $Q_{\text{loaded}} = 39\,800$ was also calculated from the energy amplitude's decay time. Off-resonance, the measured reflection is nonzero and is dominated by the waveguide facet reflection. On resonance, the light reflected from the facet interferes with the microring reflection. The model fitted to the measurement results considers this interference and accurately models the on- and off-resonance reflection spectra as shown in Fig. 5.

5.1. Large Signal Modulation Response

To observe the nonlinear response of the microring resonator and compare it with the model introduced in Section 4, we measured the temporal dynamics of the transmitted and reflected signals for high-power large signal modulation of the laser power. The tunable laser was detuned from the microring's resonant wavelength by 40 pm (see Fig. 5), and its output was modulated with 50% duty cycle and 100% modulation depth. The EDFA average output power was set to 16 dBm, resulting in an average input power to the device of $P_{\text{in}} = 12.5$ mW. The measured transmitted,

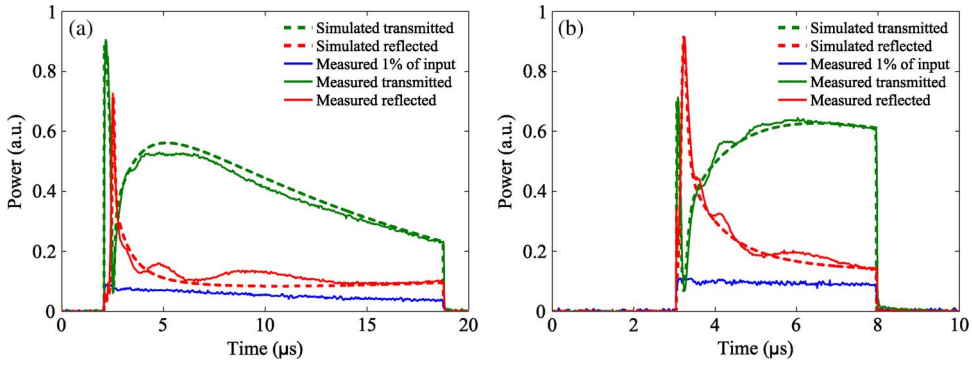

Fig. 6. Measured and simulated transmitted, reflected, and 1% of input signal powers as a function of time for a modulated laser input for modulation frequency of (a) 30 kHz and (b) 100 kHz.

reflected, and input monitor signals for the device of Fig. 5 are depicted in Fig. 6. The laser light modulation frequency is 30 kHz in Fig. 6(a) and 100 kHz in Fig. 6(b). During the on-time of the laser modulation period, the temperature of the microring's core and cladding increases, and its resonant frequency red shifts. As the resonant frequency moves to larger wavelengths, it passes the laser wavelength λ_l (see Fig. 5), and a minimum in transmitted signal and a peak in the reflected signal are observed (see Fig. 6). The microring cools down during the laser off-time, and the resonant wavelength blue shifts and returns to its initial wavelength.

As the microring's resonant wavelength moves, both the stored optical energy in the microring and the generated heat vary. As a result, the generated heat and the speed of resonant wavelength movement change. The coupled thermooptical model described by (9) considers this dynamic effect. The nonlinear differential equation (9) was solved numerically, and its parameters were chosen for the best least-square fit of the simulated transmitted and reflected signals to the measured data. The TDCMT fit values from the low-power spectra of Fig. 5 were used for the optical parameters of the device (i.e., τ, κ, and κ_m). The EDFA's output was not a perfect square wave, and so, the measured 1% of the input signal was fitted to a summation of two exponential functions multiplied by a square wave and was used to determine the waveform of the power amplitude of $s_1^+(t)$, which is the driving force in (9). Simulation results found using the model with parameter values of $t_1 = 3.90$ μs, $t_2 = 0.15$ μs, $a = 3.55 \times 10^{19}$ s $\cdot$ kg^{-1} $\cdot$ m^{-2}, and $b = 1.20 \times 10^{19}$ s $\cdot$ kg^{-1} $\cdot$ m^{-2} are shown in Fig. 6 along with the measured data. The small damped oscillatory behavior observed on top of the measured data was confirmed to be due to the EDFA transient response and was not fitted for when modeling $|s_1^+(t)|^2$ by the summation of two decaying exponential functions. Nevertheless, good agreement between the model and the measurement results was achieved.

5.2. Pump-Probe Measurement

In the pump-probe measurement, a strong modulated pump is tuned to one of the microring's resonant wavelengths (λ_1) and periodically heats up the device during its on-time. A weak CW probe signal from another laser is tuned to another resonant wavelength (λ_2) of the microring and measures the temporal response of the transmission at that wavelength. The pump laser was modulated with 10-kHz modulation frequency, 50% duty cycle, and 100% modulation depth, and was amplified using an EDFA. The lights from the two lasers were combined and coupled to a microring resonator. To block the EDFA's spontaneous emission noise, the transmitted signal was filtered using a bandpass filter centered on the probe wavelength. In contrast to the direct measurement technique presented in Section 5.1, the pump-probe technique reveals the thermooptical dynamics of the microring when it is cooling down, and thus, it is not sensitive to the pump waveform during its on-time. The setup used for this measurement is shown in Fig. 7. A microring resonator different from the one used in Section 5.1 was used for pump-probe measurement. For the device used in this measurement, the least-square TDCMT fit values were found as $\tau = 102.4$ ps, $\kappa = 1.36 \times 10^5$ s$^{-1/2}$, and $\kappa_m = 8.55 \times 10^9$ s^{-1}.

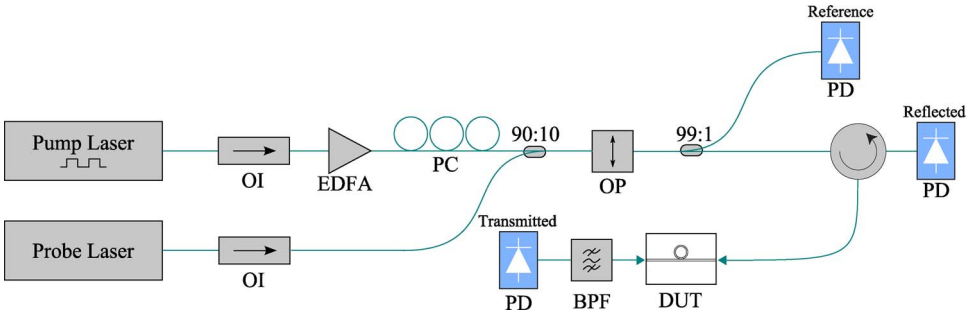

Fig. 7. Setup for the pump-probe measurement.

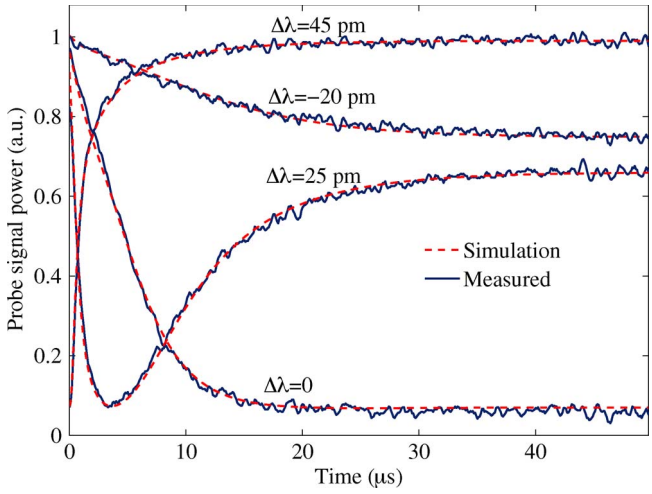

Fig. 8. Measured and simulated power of the probe signal during the pump's off time. The time is measured from the pump's turn off edge.

The measured probe signal's power during the pump's off-time for different detunings of the probe's wavelength from the device's resonant wavelength $(\Delta\lambda = \lambda_{probe} - \lambda_2)$ is shown in Fig. 8. At time $= 0$, the pump signal turns off, and the transmission spectrum, which was initially red shifted due to the heating from the pump, starts to blue shift as the device cools. Thus, different waveforms are obtained for different detunings $(\Delta\lambda)$ of the probe laser wavelength from the resonant wavelength as the entire spectrum blue shifts. The variation in the probe signal shows how the resonant frequency of the microring moves as the device cools. The results from the simulation using the coupled thermooptical model for fit model parameters of $t_1 = 7.5\ \mu$s, $t_2 = 0.5\ \mu$s, and $a/b = 1.8$ are overlaid on the measurement results in Fig. 8. The good agreement between the measured data and the simulated results suggests the validity of the proposed theoretical model.

6. Conclusion

We presented a coupled thermooptical model for modeling the temporal dynamics of self-heating in microring resonators. The time-domain model is composed of two parts, optical and thermal, which are mutually coupled to each other through the self-heating and the thermooptic effects. An adiabatic approximation of TDCMT was used for modeling the temporal optical response of mode coupling in the microrings, while a second-order lumped capacitance model described their dynamic thermal response. The final result is a nonlinear second-order differential equation for the change in the resonant frequency of microrings. The validity of the coupled thermooptical model was investigated by comparing its simulation results with two sets of experimental results obtained

from high input power measurements of Si_3N_4 microrings. One of the applications of the proposed model is in predicting the transient and steady-state responses of laser diodes with reflective microrings as cavity mirrors. The nonlinear response and resulting bistable behavior of the reflective microring resonators may affect the transient, modulation, and tuning performance of these diode lasers. We also expect the nonlinear reflection to influence the laser's amplitude and phase noise. In particular, the proposed model can be used for finding the small signal frequency response of self-heating and determining its effect on the laser's lineshape and linewidth.

References

[1] H. M. Gibbs, *Optical Bistability: Controlling Light With Light*. New York: Academic, 1985.
[2] P. Sun and R. M. Reano, "Low-power optical bistability in a free-standing silicon ring resonator," *Opt. Lett.*, vol. 35, no. 8, pp. 1124–1126, Apr. 2010.
[3] X. Zheng, Y. Luo, G. Li, I. Shubin, H. Thacker, J. Yao, K. Raj, J. E. Cunningham, and A. V. Krishnamoorthy, "Enhanced optical bistability from self-heating due to free carrier absorption in substrate removed silicon ring modulators," *Opt. Exp.*, vol. 20, no. 10, pp. 11478–11486, May 2012.
[4] M. Soltani, Q. Li, S. Yegnanarayanan, and A. Adibi, "Improvement of thermal properties of ultra-high Q silicon microdisk resonators," *Opt. Exp.*, vol. 15, no. 25, pp. 17305–17312, Dec. 2007.
[5] V. Raghunathan, S. Grillanda, V. Singh, A. Canciamilla, F. Morichetti, A. Agarwal, J. Michel, A. Melloni, and L. C. Kimerling, "Trimming of athermal silicon resonators," presented at the Integrated Photonics Research, Silicon Nanophotonics—OSA Tech. Dig., Colorado Springs, CO, Jun. 2012, Paper IW4C.5.
[6] V. R. Almeida and M. Lipson, "Optical bistability on a silicon chip," *Opt. Lett.*, vol. 29, no. 20, pp. 2387–2389, Oct. 2004.
[7] G. Priem, P. Dumon, W. Bogaerts, D. Van Thourhout, G. Morthier, and R. Baets, "Optical bistability and pulsating behaviour in silicon-on-insulator ring resonator structures," *Opt. Exp.*, vol. 13, no. 23, pp. 9623–9628, Nov. 2005.
[8] K. Ikeda, R. E. Saperstein, N. Alic, and Y. Fainman, "Thermal and Kerr nonlinear properties of plasma-deposited silicon nitride/silicon dioxide waveguides," *Opt. Exp.*, vol. 16, no. 17, pp. 12 987–12 994, Aug. 2008.
[9] A. Arbabi, P. Lu, B. G. Griffin, and L. Goddard, "Thermally-induced nonlinearity and optical bistability in Si_3N_4 microring resonators," presented at the CLEO: QELS-Fundamental Science—OSA Tech. Dig., San Jose, CA, May 2012, Paper JW4A.90.
[10] M. Notomi, A. Shinya, S. Mitsugi, G. Kira, E. Kuramochi, and T. Tanabe, "Optical bistable switching action of Si high-Q photonic-crystal nanocavities," *Opt. Exp.*, vol. 13, no. 7, pp. 2678–2687, Apr. 2005.
[11] Y. M. Kang, A. Arbabi, and L. L. Goddard, "Engineering the spectral reflectance of microring resonators with integrated reflective elements," *Opt. Exp.*, vol. 18, no. 16, pp. 16813–16825, Aug. 2010.
[12] A. Arbabi, Y. M. Kang, C. Lu, E. Chow, and L. L. Goddard, "Realization of a narrowband single wavelength microring mirror," *Appl. Phys. Lett.*, vol. 99, no. 9, pp. 091105-1–091105-3, Aug. 2011.
[13] Y. M. Kang, A. Arbabi, and L. L. Goddard, "A microring resonator with an integrated Bragg grating: A compact replacement for a sampled grating distributed Bragg reflector," *Opt. Quantum Electron.*, vol. 41, no. 9, pp. 689–697, Jul. 2009.
[14] H. A. Haus, *Waves and Fields in Optoelectronics*. Englewood Cliffs, NJ: Prentice-Hall, 1984.
[15] B. Little, S. Chu, H. Haus, J. Foresi, and J.-P. Laine, "Microring resonator channel dropping filters," *J. Lightw. Technol.*, vol. 15, no. 6, pp. 998–1005, Jun. 1997.